Control of thermoelectric properties in Mn-substituted Fe_2TiSi epilayers

Y. Shimanuki,[1] S. Yamada,[2,1] A. Masago,[2] T. Ishibe,[1] K. Kudo,[1] Y. Nakamura,[1] and K. Hamaya[2,1,*]

[1]*Department of Systems Innovation, Graduate School of Engineering Science, Osaka University, Toyonaka, Osaka 560-8531, Japan*

[2]*Center for Spintronics Research Network, Graduate School of Engineering Science, Osaka University, Toyonaka, Osaka 560-8531, Japan*

(Received 21 April 2020; revised 24 June 2020; accepted 21 July 2020; published 4 August 2020)

We experimentally study the Mn substitution effect on thermoelectric properties in a full-Heusler alloy, Fe_2TiSi. By employing molecular beam epitaxy, homogeneous and $L2_1$-ordered $Fe_2Ti_{1-x}Mn_xSi$ epilayers are achieved. The lattice constant, the saturation magnetic moment, and electrical resistivity are intentionally controlled with increasing Mn substitution. Notably, we find that the sign of the Seebeck coefficient is varied from positive to negative at around $x = 0.2$. On the basis of the first-principles calculations, we qualitatively understand that the observed variation in the electrical and thermoelectric properties arises from the change in the electronic band structure near the Fermi level, dominated by Fe and Mn atoms in $Fe_2Ti_{1-x}Mn_xSi$.

DOI: 10.1103/PhysRevB.102.054203

I. INTRODUCTION

Since the discovery of Heusler alloys [1,2], various functionalities have been explored in the field of solid-state and condensed-matter physics. In particular, "full-Heusler" alloys with the chemical formula X_2YZ have received attention, where X and Y are transition metals and Z is a main group element. In general, if the crystal structure is Cu_2MnAl ($L2_1$) type ($Fm\bar{3}m$), the lattice points occupying the X, Y, and Z elements in full-Heusler alloys can be called (A,C), B, and D sites. A semimetallic full-Heusler alloy, Fe_2VAl, has been studied as a next-generation thermoelectric material containing nontoxic elements [3–8], in which Fe_2VAl is an $L2_1$-type crystal structure. One of the unique features in Fe_2VAl is controllable physical properties by changing the electronic band structures or shifting the position of the Fermi level E_F [5,6,8]. In particular, because $L2_1$-ordered Fe_2VAl has a sharp pseudogap at E_F [4,9–18], electrical and thermoelectric properties such as the electrical resistivity ρ and Seebeck coefficient S were intentionally modulated by changing the chemical composition or substituting constituent elements [5,6,8], leading to an improvement in the thermoelectric performance [19].

Recently, as a semiconducting full-Heusler alloy, Fe_2TiSi was theoretically proposed by Yabuuchi *et al.* [20]. The predicted S values of Fe_2TiSi are from -160 to -350 μV/K, one order of magnitude larger than those of Fe_2VAl ($S \sim 40$ μV/K) at 300 K [5–7]. Namely, from the viewpoint of S, Fe_2TiSi is expected to be one of the high-performance thermoelectric materials with nontoxic elements [20]. Although the synthesis of bulk Fe_2TiSi was attempted long before the prediction in Ref. [20], the phase separation, including some other phases such as hexagonal Fe_2Ti, easily occurred [21,22]. In 2014 Meinert *et al.* demonstrated epitaxial growth of Fe_2TiSi films and examined their electric and magnetic properties [23]. Very recently, we achieved a stoichiometric, homogeneous, and single-crystalline Fe_2TiSi epilayer and clarified the room-temperature S and thermal conductivity κ values of 101 μV/K and 5.6 W/(m K), respectively [24]. However, controlling the physical properties, including the thermoelectric properties, has never been explored.

In this paper, we study the Mn substitution effect on the thermoelectric properties in Fe_2TiSi epilayers. By employing molecular beam epitaxy, homogeneous and $L2_1$-ordered $Fe_2Ti_{1-x}Mn_xSi$ epilayers are experimentally achieved. The lattice constant, the saturation magnetic moment, and the electrical resistivity are intentionally controlled by increasing the Mn substitution x. Notably, we find that the sign of the Seebeck coefficient is varied from positive to negative at around $x = 0.2$. On the basis of the first-principles calculations, we propose that the observed variation in the electrical and thermoelectric properties arises from the change in the electronic band structure near E_F, dominated by Fe and Mn atoms in $Fe_2Ti_{1-x}Mn_xSi$.

II. EXPERIMENTAL AND COMPUTATIONAL DETAILS

$Fe_2Ti_{1-x}Mn_xSi$ ($x = 0$, 0.23, 0.41, 0.58, and 0.87) epilayers with a thickness of ~50 nm were grown on spinel-type $MgAl_2O_4(001)$ substrates (sample size: 1×1 cm^2) by molecular beam epitaxy (MBE) with nonstoichiometric deposition techniques [7,8,24–30]. Because the lattice constants of Fe_2TiSi and Fe_2MnSi are ~0.576 nm [24] and 0.5654–0.5672 nm [25,31–33], respectively, we can roughly expect the lattice constant of $Fe_2Ti_{1-x}Mn_xSi$ between them. Thus, the mismatch between the expected lattice constant and half of the diagonal length of the lattice constant of $MgAl_2O_4$ ($1/\sqrt{2} \times 0.8083$ nm $= 0.5715$ nm) is less than 2%. After loading the $MgAl_2O_4(001)$ substrates into the MBE chamber with a base pressure of $\sim 10^{-7}$ Pa, a heat treatment at 600 °C for 1 h was performed. From *in situ* reflection high-energy electron diffraction (RHEED) observations (not shown here), the good flatness of the $MgAl_2O_4(001)$ surface was confirmed. Cooling the substrate temperature down to 350 °C, we grew $Fe_2Ti_{1-x}Mn_xSi$ layers by coevaporating Fe, Ti, Mn, and Si using Knudsen cells [24,25]. After the

*hamaya@ee.es.osaka-u.ac.jp

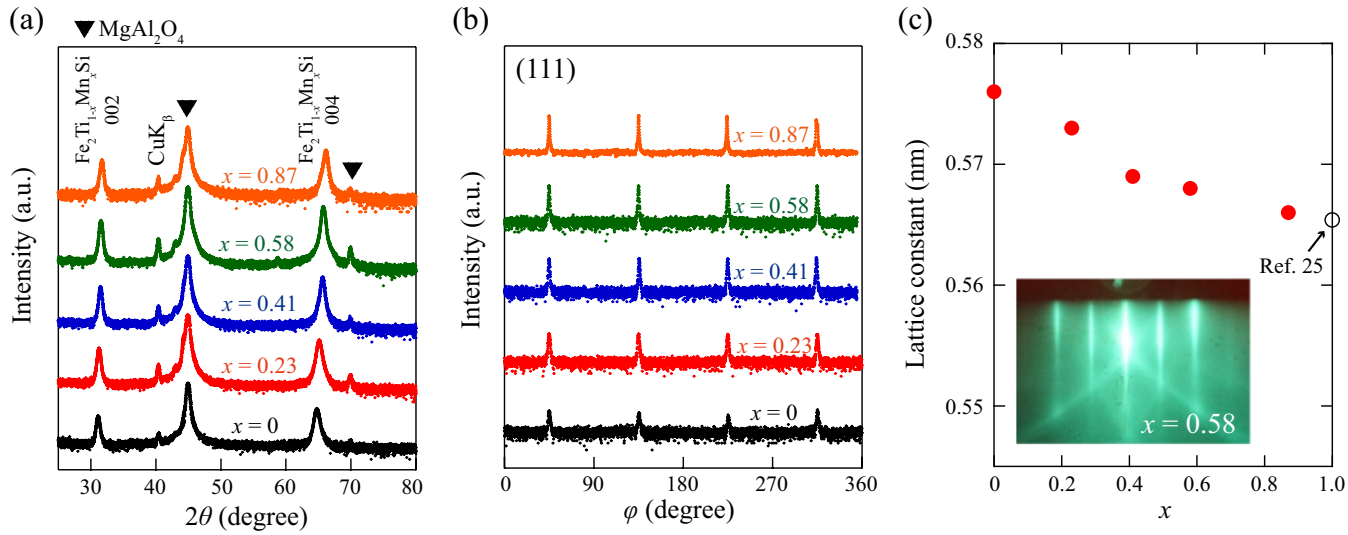

FIG. 1. (a) θ-2θ XRD patterns for the $Fe_2Ti_{1-x}Mn_xSi$ epilayers. (b) ϕ-scan measurements of the (111) plane for the $Fe_2Ti_{1-x}Mn_xSi$ epilayers. (c) The lattice constant of the $Fe_2Ti_{1-x}Mn_xSi$ epilayers estimated from (a). The inset shows the RHEED pattern for the $Fe_2Ti_{0.42}Mn_{0.58}Si$ layer grown at 350 °C.

growth, structural characterizations were conducted by *in situ* RHEED, x-ray diffraction (XRD), high-angle annular dark-field scanning transmission electron microscopy (HAADF-STEM), and energy dispersive x-ray spectroscopy (EDX) measurements. Magnetic properties were measured by using a vibrating sample magnetometer at various temperatures.

To measure the electrical properties, the grown $Fe_2Ti_{1-x}Mn_xSi$ epilayers were patterned into 80-μm-wide and 400-μm-long Hall-bar devices by conventional photolithography and Ar^+ ion-milling techniques. Electrical transport measurements were performed by a standard four-point-probe dc method at various temperatures. For the evaluation of the Seebeck coefficient S, we used a conventional system allowing thermoelectromotive force and temperature difference measurement [34,35]. Here, because the $MgAl_2O_4$ substrate was an insulator with an extremely large sheet resistance ($> 10^7$ Ω/square), the measured S corresponds to that of the $Fe_2Ti_{1-x}Mn_xSi$ epilayers with a relatively small sheet resistance of 10^2–10^3 Ω/square.

To understand electronic band structures in $Fe_2Ti_{1-x}Mn_xSi$, we also conducted first-principles density-functional theory (DFT) calculations with the AKAI-KKR package [36], where the package is based on the Korringa-Kohn-Rostoker method [37] with a coherent potential approximation. In this study, the following conditions are assumed: the Perdew-Burke-Ernzerhof functional is used for the exchange-correlation calculations [38,39], there are 413 k-sampling points, and the experimentally obtained lattice constant was used. In addition, for qualitatively evaluating the change in the Seebeck coefficient in $Fe_2Ti_{1-x}Mn_xSi$, the following semiclassical Boltzmann transport formalism within the constant relaxation time approximation was used [40,41]:

$$S(T) = -\frac{1}{|e|T}\frac{\int_{-\infty}^{\infty} D(\epsilon)(\epsilon-\mu)\left(-\frac{\partial F(\epsilon,T)}{\partial \epsilon}\right)d\epsilon}{\int_{-\infty}^{\infty} D(\epsilon)\left(-\frac{\partial F(\epsilon,T)}{\partial \epsilon}\right)d\epsilon}, \quad (1)$$

where e is the unit charge of an electron, μ is the chemical potential, ϵ is the energy, $F(\epsilon, T)$ is the Fermi-Dirac distribution function, and $D(\epsilon)$ is the electron's density of states (DOS). In the numerical calculations based on this theory, the above formula via assumptions, which are the relaxation time approximation and the energy-insensitive group velocity, is often used [40,41].

III. RESULTS

A. Substitution of Mn for Ti in Fe_2TiSi

A representative RHEED image of the surface of an $Fe_2Ti_{0.42}Mn_{0.58}Si$ ($x = 0.58$) layer after growth is presented in the inset of Fig. 1(c). From these RHEED observations, good two-dimensional epitaxial growth was indicated for all x of $Fe_2Ti_{1-x}Mn_xSi$. Figure 1(a) shows θ-2θ XRD patterns for the $Fe_2Ti_{1-x}Mn_xSi$ layers. Except for the peaks derived from the $MgAl_2O_4$ substrate, only 002 and 004 diffraction peaks from the $Fe_2Ti_{1-x}Mn_xSi$ layers are clearly seen at 2θ of $\sim 31^\circ$ and $\sim 65^\circ$, respectively. This feature indicates the formation of (001)-oriented $Fe_2Ti_{1-x}Mn_xSi$ epilayers on $MgAl_2O_4$. In addition, ϕ-scan measurements for various x are presented in Fig. 1(b). For all x, (111) diffraction peaks with fourfold symmetry are clearly observed, indicating the presence of the $L2_1$-ordered structure of a full-Heusler alloy. The lattice constant estimated from the XRD data in Fig. 1(a) is summarized in Fig. 1(c), together with the value of the lattice constant of an Fe_2MnSi epilayer [25]. With increasing x, the lattice constant decreases almost linearly, following the size of the atomic radius of Ti and Mn (Ti > Mn). This behavior implies that the substitution of Mn for Ti in Fe_2TiSi is experimentally demonstrated.

We further perform the characterizations by HAADF-STEM and EDX. Figures 2(a) and 2(b) show a typical HAADF-STEM image with an enlarged one near the interface and EDX mapping images of each element, respectively, for the $Fe_2Ti_{0.42}Mn_{0.58}Si$ epilayer. EDX line profiles

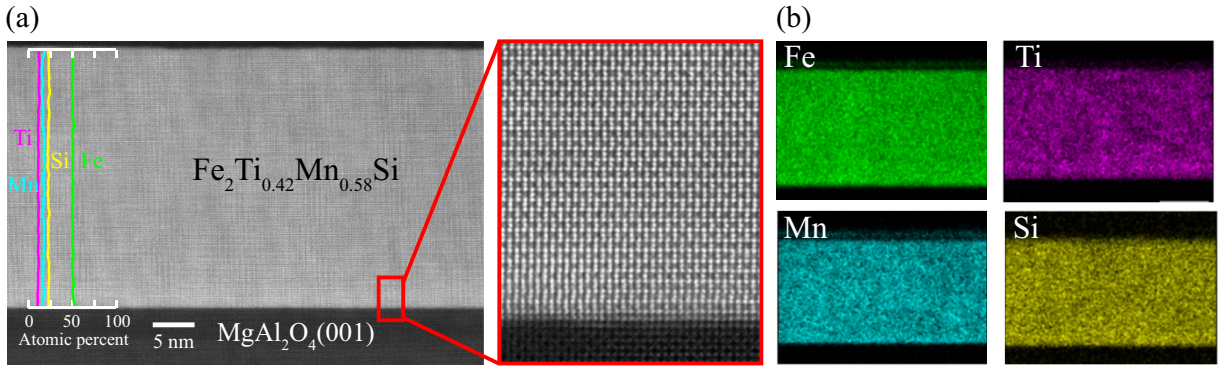

FIG. 2. (a) HAADF-STEM image with EDX line profiles of $Fe_2Ti_{0.42}Mn_{0.58}Si/MgAl_2O_4(001)$ and an enlarged image near the interface. (b) EDX elemental maps for $Fe_2Ti_{0.42}Mn_{0.58}Si/MgAl_2O_4(001)$.

of the $Fe_2Ti_{0.42}Mn_{0.58}Si$ epilayer are presented in Fig. 2(a). The contrast of the HAADF-STEM image is nearly uniform over the measured area, and the atomic composition fluctuation in the constituent elements cannot be seen from the EDX mappings. From these data, we can judge that the $Fe_2Ti_{0.42}Mn_{0.58}Si$ epilayer on $MgAl_2O_4(001)$ is uniformly grown and there is no phase separation in the film, which is similar to the nonsubstituted Fe_2TiSi epilayers previously shown in Ref. [24]. Notably, periodic contrasts indicating the formation of the $L2_1$-ordered structure are clearly observed in the enlarged image near the interface. This means that the $L2_1$-ordered structure, already detected in XRD ϕ-scan measurements in Fig. 1(b), is realized in the vicinity of the interface between the epilayer and the substrate. Given these structural characterizations in Figs. 1 and 2, we conclude that the Mn-substituted $Fe_2Ti_{1-x}Mn_xSi$ epilayers are experimentally obtained by MBE techniques.

B. Magnetic properties

Although Fe_2TiSi was theoretically predicted to be a nonmagnetic material [20], the obtained Fe_2TiSi film had 6% Fe ⇔ Ti disordering, causing the presence of the small magnetic moments in our previous work [24]. To further understand the quality of the grown $Fe_2Ti_{1-x}Mn_xSi$ epilayers, we investigate its magnetic properties, as shown in the inset of Fig. 3(a). The field-dependent magnetization curves at 10 K evidently show the increase in the magnetic moments with increasing Mn substitution x. Since Fe_2MnSi is well known to be a ferromagnetic material with a Curie temperature of ∼230 K [25,32,33], the observed finite magnetic moments for the $Fe_2Ti_{1-x}Mn_xSi$ epilayers are affected by the Mn substitution in Fe_2TiSi. Thus, we should compare the experimental data with theoretical data.

In the main panel of Fig. 3(a), we summarize the saturation magnetic moment M_S versus x at 10 K (blue triangles), together with the calculated values of $Fe_2Ti_{1-x}Mn_xSi$ with the presence of 6% Fe ⇔ Ti disordering (red circles) [24]. In the calculation, the Ti concentration of 6% means the average percent of the substituted Ti atoms for Fe atoms at the (A,C) sites. In Fig. 3(a) the values of M_S (blue triangles) are systematically changed with increasing x for $x \leqslant 0.58$, very consistent with the calculated values (red circles) including the 6% Fe ⇔ Ti disordering, except for $x = 0.87$. In the case of $x = 0.87$, because we have to consider that the B site of Ti in Fe_2TiSi is majorly substituted for Mn, the influence of Fe ⇔ Mn disordering on the magnetic properties should

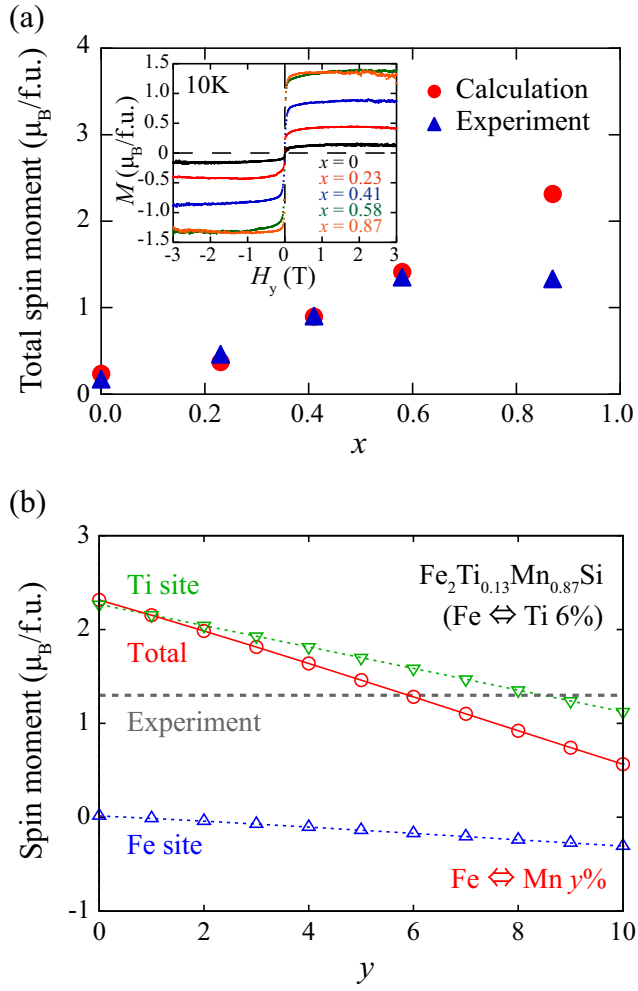

FIG. 3. (a) Calculated total spin moment of $Fe_2Ti_{1-x}Mn_xSi$ with the presence of 6% Fe ⇔ Ti disordering (red circles) and the experimental data of $Fe_2Ti_{1-x}Mn_xSi$ epilayers at 10 K (blue triangles). The inset shows M-H curves for $Fe_2Ti_{1-x}Mn_xSi$ epilayers at 10 K. (b) Total and local spin moments of $Fe_2Ti_{0.13}Mn_{0.87}Si$ as a function of y (Fe ⇔ Mn disordering concentration) with the presence of 6% Fe ⇔ Ti disordering. The gray dashed line indicates the experimental data of $Fe_2Ti_{0.13}Mn_{0.87}Si$ epilayers at 10 K.

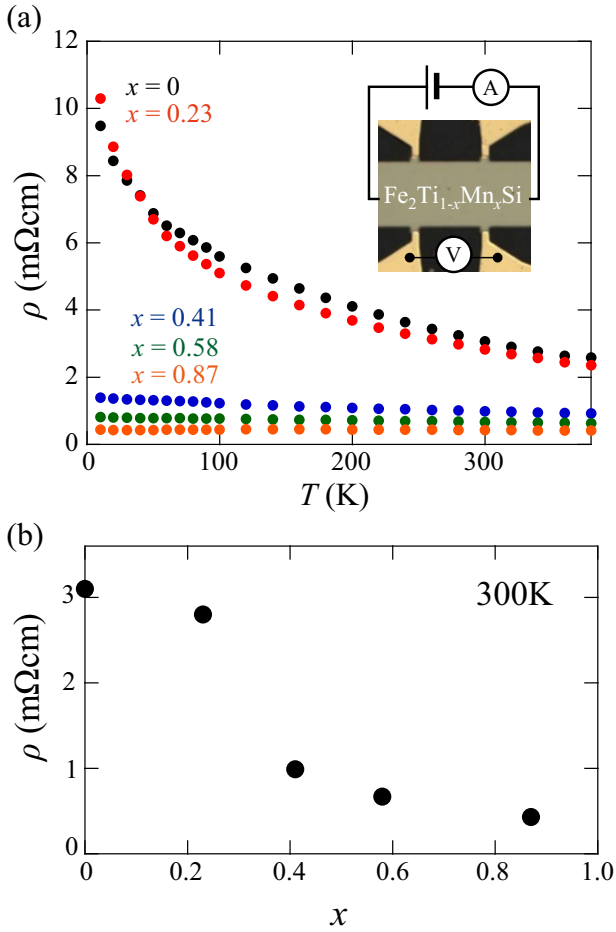

FIG. 4. (a) Temperature dependence of ρ for the $Fe_2Ti_{1-x}Mn_xSi$ epilayers. The inset shows a micrograph of the fabricated Hall-bar device. (b) The values of ρ at 300 K as a function of x in the $Fe_2Ti_{1-x}Mn_xSi$ epilayers.

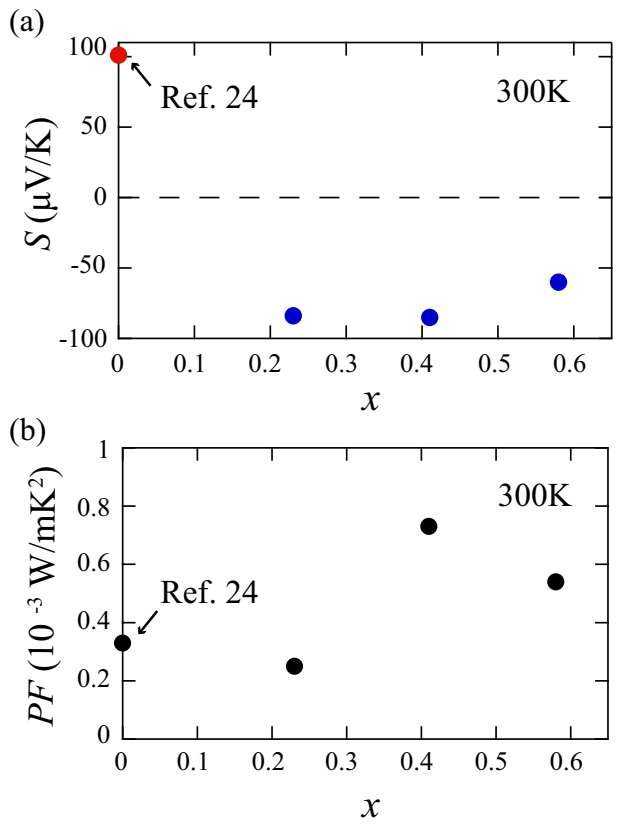

FIG. 5. Room-temperature (a) Seebeck coefficient S and (b) power factor (PF) of the grown $Fe_2Ti_{1-x}Mn_xSi$ epilayers.

be included. Figure 3(b) shows the calculated total and local spin moments (μ_B/f.u.) of $Fe_2Ti_{0.13}Mn_{0.87}Si$ versus y with the presence of 6% Fe ⇔ Ti disordering, where y is the percentage of the Fe ⇔ Mn disordering considered here. The gray dashed line indicates the experimental data of the $Fe_2Ti_{0.13}Mn_{0.87}Si$ epilayer at 10 K. When the value of y is increased, the total spin moment tends to decrease monotonically. Notably, at $y \sim 6$, the experimental value of M_S is very consistent with the calculated one. Therefore, we interpret that heavily Mn substituted Fe_2TiSi epilayers have a small amount of Fe ⇔ Mn disordering in addition to the Fe ⇔ Ti disordering.

C. Electrical and thermoelectric properties

Figure 4(a) shows the temperature dependence of the electrical resistivity ρ of the $Fe_2Ti_{1-x}Mn_xSi$ epilayers with various x by measuring four-point-probe voltages with Hall-bar devices, as shown in the inset. While the value of ρ increases largely with decreasing temperature for $x = 0.23$, similar to that in Fe_2TiSi [24], the behavior changes dramatically after the substitution of Mn for $x \geqslant 0.41$; the value of ρ is almost independent of temperature. The values of ρ at 300 K as a function of x are summarized in Fig. 4(b). With increasing x, the values of ρ at 300 K decrease, indicating an intentional control of ρ at room temperature by varying x. Similar changes in ρ have frequently been observed in Fe_2VAl with the substitution of other elements for V or Al [5,6,8,19]. Therefore, electrical properties of the Mn-substituted Fe_2TiSi can be interpreted in terms of the shift of the position of E_F or the variation of the electronic band structures in Fe_2TiSi. A possible mechanism is discussed later.

To evaluate the thermoelectric properties of the Mn-substituted Fe_2TiSi, we plot the value of S versus x at 300 K in Fig. 5(a), together with that for Fe_2TiSi ($x = 0$) [24]. We note that the sign of S changes from positive to negative after the substitution of Mn for $x \geqslant 0.23$, meaning that the thermal transport in the $Fe_2Ti_{1-x}Mn_xSi$ epilayers can be experimentally modulated by substituting constituent elements, in addition to Fe_2VAl [5,6,8,19]. However, the magnitude of S is not systematically changed with increasing the Mn substitution x. We find that, even after the Mn substitution, the relatively large S of -60 to -85 μV/K is maintained.

Using the values of ρ and S shown in Figs. 4(b) and 5(a), respectively, we estimate the magnitude of the power factor (PF $= S^2/\rho$) at 300 K in Fig. 5(b). Because of the marked decrease in ρ for $x = 0.41$, the largest value of PF is estimated to be 0.72 (10^{-3} W/mK^2). We summarize comparisons of ρ, S, and PF at 300 K in Table I among $Fe_2Ti_{0.59}Mn_{0.41}Si$ (this work), Fe_2TiSi [24], $Fe_2VAl_{0.57}Si_{0.43}$ [8], and Fe_2VAl [7] epilayers, grown by MBE at 350 °C. Consequently, the value of PF at 300 K for the $Fe_2Ti_{0.59}Mn_{0.41}Si$ epilayer is more than

TABLE I. Comparison of ρ, S, and PF at 300 K among $Fe_2Ti_{0.59}Mn_{0.41}Si$ (this study), Fe_2TiSi [24], $Fe_2VAl_{0.57}Si_{0.43}$ [8], and Fe_2VAl [7] epilayers.

	$Fe_2Ti_{0.59}Mn_{0.41}Si$ (this study)	Fe_2TiSi [24]	$Fe_2VAl_{0.57}Si_{0.43}$ [8]	Fe_2VAl [7]
Ordering	$L2_1$	$L2_1$	$L2_1$	$L2_1$
ρ (mΩ cm)	1.0	3.1	0.47	1.4
S (μV/K)	−85	+101	−64	+40
PF (10^{-3} W/mK^2)	0.72	0.33	0.87	0.11

twice as large as that for the nonsubstituted Fe_2TiSi epilayer. From these results, we clarify that the Mn substitution enables us to enhance the thermoelectric performance of Fe_2TiSi. Assuming that the value of κ at 300 K for the $Fe_2Ti_{0.59}Mn_{0.41}Si$ epilayer is the same as that for the nonsubstituted Fe_2TiSi epilayer (∼5.6 W/m K)[24], we can estimate the dimensionless figure of merit, $ZT = S^2T/(\rho\kappa)$, to be ∼0.039 (at 300 K), smaller than that for the $Fe_2VAl_{0.57}Si_{0.43}$ epilayer [8]. The low ZT value estimated here is attributed to relatively high values of ρ compared to those of $Fe_2VAl_{0.57}Si_{0.43}$. Up to now, because of experimental difficulties with the synthesis of bulk Fe_2TiSi [21,22], there has been no report on the control of the thermoelectric properties of Fe_2TiSi. The results proved in this study are attributed to the experimental achievement of the substitution of Mn for Ti in homogeneous and single-crystalline Fe_2TiSi epilayers.

IV. DISCUSSION

While the substitution of Mn for Ti in Fe_2TiSi generally corresponds to the electron doping because the number of valence electrons of Mn is larger than that of Ti, the substitution

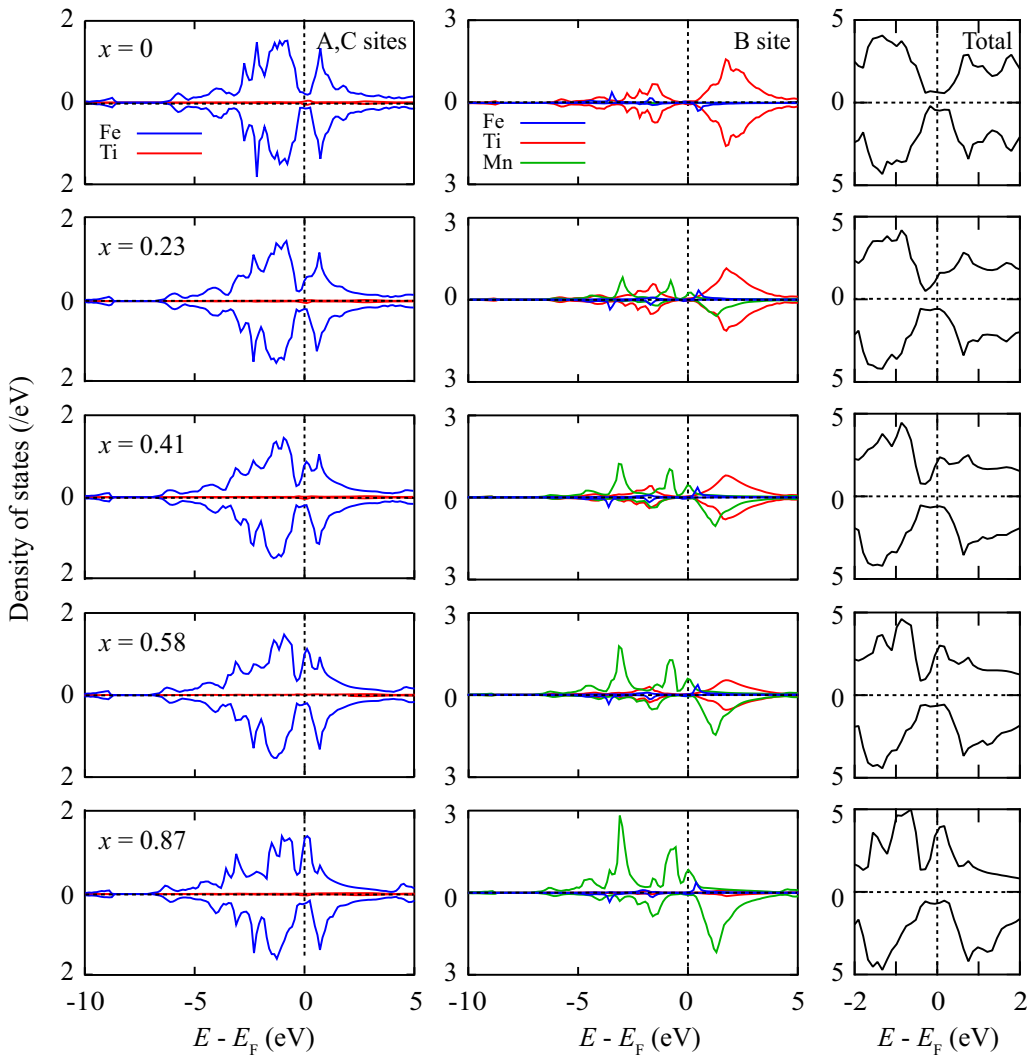

FIG. 6. Spin-resolved partial density of states (DOS) at the (A,C) sites (left column) and at the B site (middle column) of $Fe_2Ti_{1-x}Mn_xSi$ with the presence of 6% Fe ⇔ Ti disordering. The right column shows the total DOS near the Fermi level. We assumed that Mn atoms occupy only the B site.

of the B site in full-Heusler alloys can affect the electronic band structures. Therefore, we discuss the Mn substitution effect on the electronic band structures in $Fe_2Ti_{1-x}Mn_xSi$ using first-principles DFT calculations. Here the lattice constant is changed from 0.576 to 0.566 nm based on the experimental value shown in Fig. 1(c). Figure 6 displays the spin-resolved partial DOS at the (A,C) sites (left column) and at the B site (middle column) of $Fe_2Ti_{1-x}Mn_xSi$ for various x (Mn substitution). Here, for all the calculations, we are dealing with the presence of the 6% Fe $\Leftrightarrow$ Ti disordering [24] in $Fe_2Ti_{1-x}Mn_xSi$, and the substituted Mn atoms occupy only the B site in the full-Heusler structure. Because there is only 6% of the Ti atoms at the (A,C) sites, the contribution of the Ti atoms to the (A,C) sites is negligibly small compared with Fe atoms. For $x = 0$ (Fe_2TiSi), the DOS derived from Fe atoms at the (A,C) site forms at around E_F. It was reported that the observed impuritylike state in the band gap originates from the 6% Fe $\Leftrightarrow$ Ti disordering in Fe_2TiSi [24]. Notably, there is almost no influence of the DOS derived from Ti atoms in both the (A,C) and B sites on the state at around E_F for $x = 0$ (Fe_2TiSi).

With increasing x, the electronic band structures dramatically vary. For $x = 0.23$, the additional DOS is gradually observed near E_F in the majority spins of Fe atoms at the (A,C) sites, and it becomes a spin-polarized DOS like a ferromagnetic metal for $x \geqslant 0.41$. This feature is consistent with the experimental data. For the majority spins at the B site, the DOS derived from Mn atoms is increased with increasing x, and near E_F it becomes a half metal for $x \geqslant 0.23$. Since it is well known that Fe_2MnSi becomes a half-metallic ferromagnet [25,31–33], the observed feature with increasing x is reasonable. As described above, the contribution of Ti to the DOS near E_F is very small for all x in both the (A,C) and B sites of $Fe_2Ti_{1-x}Mn_xSi$. Namely, we infer that the observed electrical and thermoelectric properties in Figs. 4 and 5 are predominantly determined by Fe atoms at the (A,C) sites and the substituted Mn atoms at the B site.

Finally, using the semiclassical Boltzmann transport formalism shown in Eq. (1), we qualitatively evaluate the change in S from positive to negative by increasing x for $Fe_2Ti_{1-x}Mn_xSi$. Here S values calculated from Eq. (1) can deviate from the experimental values because of simple assumptions: chemical potentials fixed at the band edge, no magnon effects, and the relaxation time approximation [40,41]. In addition, although theoretical calculations indicate the spin-polarized DOSs at 0 K, the actual $Fe_2Ti_{1-x}Mn_xSi$ films are nonmagnetic at room temperature. Thus, to discuss the thermoelectric properties based on the calculated DOSs at room temperature, the deviations between theory and experiment should be considered. When x is increased from 0 to 0.23 and $\mu \sim 6$ meV, the value of S can be changed from $+16.7$ to -7.5 μV/K, in which the value of S cannot be reproduced only by the semiclassical Boltzmann transport formalism [40,41]. However, the change in S from positive to negative by increasing x can tentatively be interpreted in terms of the variation in the change in the DOS near E_F. From these considerations, the electrical and thermoelectric properties of the Mn-substituted Fe_2TiSi can be understood not by the shift of the position of E_F but by the variation of the electronic band structures in Fe_2TiSi.

V. CONCLUSION

We have studied the Mn substitution effect on thermoelectric properties in Fe_2TiSi. By employing MBE, homogeneous and $L2_1$-ordered $Fe_2Ti_{1-x}Mn_xSi$ epilayers were achieved. The lattice constant, the saturation magnetic moment, and the electrical resistivity were intentionally controlled with increasing Mn substitution. We found that the sign of the Seebeck coefficient is varied from positive to negative at around $x = 0.2$ in $Fe_2Ti_{1-x}Mn_xSi$. On the basis of the first-principles calculations, we propose that the variation in the electrical and thermoelectric properties arises from the change in the electronic band structure near E_F, dominated by Fe and Mn atoms in $Fe_2Ti_{1-x}Mn_xSi$.

ACKNOWLEDGMENTS

This work was partly supported by JSPS KAKENHI (Grants No. 16H02333, No. 18KK0111, No. 18K13789, No. 19H05616, No. 19H00853), JST-CREST (Grant No. JPMJCR18J1), the TEPCO Memorial Foundation, and the Kansai Research Foundation for Technology Promotion. K.K. acknowledges JSPS Research Fellowships for Young Scientists (No. 20J10124). The computation was performed at the Supercomputer Center, Institute for Solid State Physics, University of Tokyo.

[1] F. Heusler, Verh. Dtsch. Phys. Ges. **12**, 219 (1903).
[2] T. Graf, C. Felser, and S. S. P. Parkin, Prog. Solid State Chem. **39**, 1 (2011).
[3] Y. Nishino, M. Kato, S. Asano, K. Soda, M. Hayasaki, and U. Mizutani, Phys. Rev. Lett. **79**, 1909 (1997).
[4] Y. Nishino, Mater. Trans. **42**, 902 (2001).
[5] Y. Nishino, S. Deguchi, and U. Mizutani, Phys. Rev. B **74**, 115115 (2006).
[6] C. S. Lue, C. F. Chen, J. Y. Lin, Y. T. Yu, and Y. K. Kuo, Phys. Rev. B **75**, 064204 (2007).
[7] S. Yamada, K. Kudo, R. Okuhata, J. Chikada, Y. Nakamura, and K. Hamaya, Appl. Phys. Express **10**, 115802 (2017).
[8] K. Kudo, S. Yamada, J. Chikada, Y. Shimanuki, T. Ishibe, S. Abo, H. Miyazaki, Y. Nishino, Y. Nakamura, and K. Hamaya, Phys. Rev. B **99**, 054201 (2019).
[9] G. A. Botton, Y. Nishino, and C. J. Humphreys, Intermetallics **8**, 1209 (2000).
[10] D. J. Singh and I. I. Mazin, Phys. Rev. B **57**, 14352 (1998).
[11] R. Weht and W. E. Pickett, Phys. Rev. B **58**, 6855 (1998).
[12] M. Weinert and R. E. Watson, Phys. Rev. B **58**, 9732 (1998).
[13] A. Bansil, S. Kaprzyk, P. E. Mijnarends, and J. Toboła, Phys. Rev. B **60**, 13396 (1999).
[14] S. Bandaru and P. Jund, Phys. Status Solidi B **254**, 1600441 (2017).

[15] H. Okamura, J. Kawahara, T. Nanba, S. Kimura, K. Soda, U. Mizutani, Y. Nishino, M. Kato, I. Shimoyama, H. Miura, K. Fukui, K. Nakagawa, H. Nakagawa, and T. Kinoshita, Phys. Rev. Lett. **84**, 3674 (2000).
[16] C. S. Lue and J. H. Ross, Jr., Phys. Rev. B **61**, 9863 (2000).
[17] K. Soda, T. Mizutani, O. Yoshimoto, S. Yagi, U. Mizutani, H. Sumi, Y. Nishino, Y. Yamada, T. Yokoya, S. Shin, A. Sekiyama, and S. Suga, J. Synchrotron Radiat. **9**, 233 (2002).
[18] H. Miyazaki, S. Tateishi, M. Matsunami, K. Soda, S. Yamada, K. Hamaya, and Y. Nishino, J. Electron. Spectrosc. Relat. Phenom. **232**, 1 (2019).
[19] S. Masuda, K. Tsuchiya, J. Qiang, H. Miyazaki, and Y. Nishino, J. Appl. Phys. **124**, 035106 (2018).
[20] S. Yabuuchi, M. Okamoto, A. Nishide, Y. Kurosaki, and J. Hayakawa, Appl. Phys. Express **6**, 025504 (2013).
[21] D. H. Jack and R. W. K. Honeycombe, Acta Metall. **20**, 787 (1972).
[22] V. Niculescu, T. J. Burch, K. Raj, and J. I. Budnick, J. Magn. Magn. Mater. **5**, 60 (1977).
[23] M. Meinert, M. P. Geisler, J. Schmalhorst, U. Heinzmann, E. Arenholz, W. Hetaba, M. Stöger-Pollach, A. Hütten, and G. Reiss, Phys. Rev. B **90**, 085127 (2014).
[24] Y. Shimanuki, K. Kudo, T. Ishibe, A. Masago, S. Yamada, Y. Nakamura, and K. Hamaya, J. Appl. Phys. **127**, 055106 (2020).
[25] K. Hamaya, H. Itoh, O. Nakatsuka, K. Ueda, K. Yamamoto, M. Itakura, T. Taniyama, T. Ono, and M. Miyao, Phys. Rev. Lett. **102**, 137204 (2009).
[26] K. Tanikawa, S. Oki, S. Yamada, M. Kawano, M. Miyao, and K. Hamaya, Thin Solid Films **557**, 390 (2014).
[27] S. Yamada, K. Tanikawa, S. Oki, M. Kawano, M. Miyao, and K. Hamaya, Appl. Phys. Lett. **105**, 071601 (2014).
[28] Y. Fujita, M. Yamada, M. Tsukahara, T. Oka, S. Yamada, T. Kanashima, K. Sawano, and K. Hamaya, Phys. Rev. Appl. **8**, 014007 (2017).
[29] K. Arima, F. Kuroda, S. Yamada, T. Fukushima, T. Oguchi, and K. Hamaya, Phys. Rev. B **97**, 054427 (2018).
[30] S. Yamada, S. Kobayashi, A. Masago, L. S. R. Kumara, H. Tajiri, T. Fukushima, S. Abo, Y. Sakuraba, K. Hono, T. Oguchi, and K. Hamaya, Phys. Rev. B **100**, 195137 (2019).
[31] V. Niculescu, K. Raj, T. J. Burch, and J. I. Budnick, Phys. Rev. B **13**, 3167 (1976).
[32] S. Yoon and J. G. Booth, J. Phys. F **7**, 1079 (1977).
[33] L. Hongzhi, Z. Zhiyong, M. Li, X. Shifeng, L. Heyan, Q. Jingping, L. Yangxian, and W. Guangheng, J. Phys. D **40**, 7121 (2007).
[34] T. Ishibe, A. Tomeda, K. Watanabe, Y. Kamakura, N. Mori, N. Naruse, Y. Mera, Y. Yamashita, and Y. Nakamura, ACS Appl. Mater. Interfaces **10**, 37709 (2018).
[35] S. Sakane, T. Ishibe, T. Hinakawa, N. Naruse, Y. Mera, Md. M. Alam, K. Sawano, and Y. Nakamura, Appl. Phys. Lett. **115**, 182104 (2019).
[36] H. Akai, J. Phys. Soc. Jpn. **51**, 468 (1982).
[37] J. Korringa, Physica **13**, 392 (1947); W. Kohn and N. Rostoker, Phys. Rev. **94**, 1111 (1954).
[38] J. P. Perdew, K. Burke, and M. Ernzerhof, Phys. Rev. Lett. **77**, 3865 (1996).
[39] A. Filippetti, C. D. Pemmaraju, S. Sanvito, P. Delugas, D. Puggioni, and V. Fiorentini, Phys. Rev. B **84**, 195127 (2011).
[40] C. W. Wang, Y. Y. Y. Xia, Z. Tian, J. Jiang, B. H. Li, S. T. Cui, H. F. Yang, A. J. Liang, X. Y. Zhan, G. H. Hong, S. Liu, C. Chen, M. X. Wang, L. X. Yang, Z. Liu, Q. X. Mi, G. Li, J. M. Xue, Z. K. Liu, and Y. L. Chen, Phys. Rev. B **96**, 165118 (2017).
[41] G. A. Naydenov, P. J. Hasnip, V. K. Lazarov, and M. I. J. Probert, J. Phys.: Condens. Matter. **32**, 125401 (2020).